computation in the presence of errors is ongoing, it already appears that the boson-sampling model makes less stringent demands on device performance than universal photonic quantum computers (12, 23, 29). There is thus reason for optimism that ongoing advances in integrated photonics, such as reduced transmission loss, efficient number-resolving detectors (30), and multiplexed (31, 32) or single-emitter (17) photon sources, will enable larger QBSMs that outperform classical computers. Beyond the specific boson-sampling problem, such a device would provide evidence for the computational power of quantum mechanics.

#### References and Notes

- 1. D. P. DiVincenzo, Fortschr. Phys. 48, 771 (2000).
- R. Raussendorf, H. J. Briegel, *Phys. Rev. Lett.* 86, 5188 (2001).
- 3. M. A. Nielsen, Phys. Lett. A 308, 96 (2003).
- 4. A. M. Childs, Phys. Rev. Lett. 102, 180501 (2009).
- 5. P. Walther et al., Nature 434, 169 (2005).
- C.-Y. Lu, D. E. Browne, T. Yang, J.-W. Pan, *Phys. Rev. Lett.* 99, 250504 (2007).
- 7. B. P. Lanyon et al., Science 334, 57 (2011).
- 8. E. Lucero et al., Nat. Phys. 8, 719 (2012).
- 9. E. Knill, R. Laflamme, *Phys. Rev. Lett.* **81**, 5672 (1998)
- 10. S. P. Jordan, Quant. Inf. Comput. 10, 470 (2010).
- D. Shepherd, M. J. Bremner, Proc. R. Soc. London Ser. A 465, 1413 (2009).

- S. Aaronson, A. Arkhipov, "The computation complexity of linear optics," in *Proceedings of the 43rd Annual ACM Symposium on the Theory of Computing* (STOC'11), San Jose, CA, 6 to 8 June 2011 (Association for Computing Machinery, New York, 2011), pp. 333–342.
- 13. Materials and methods are available as supplementary materials on *Science* Online.
- 14. E. Caianiello, Nuovo Cim. 10, 1634 (1953).
- L. Troyansky, N. Tishby, "Permanent uncertainty: on the quantum evaluation of the determinant and the permanent of a matrix," in *Proceedings of Physics and Computation* (PhysComp 96), Boston, MA, 22 to 24 Nov 1996 (New England Complex Systems Institute, Cambridge, MA, 1996), pp. 314–318.
- 16. L. G. Valiant, Theor. Comput. Sci. 8, 189 (1979).
- M. D. Eisaman, J. Fan, A. Migdall, S. V. Polyakov, *Rev. Sci. Instrum.* 82, 071101 (2011).
- 18. B. J. Metcalf et al., Nat. Commun. 4, 1356 (2012).
- B. J. Smith, D. Kundys, N. Thomas-Peter, P. G. R. Smith,
   I. A. Walmsley, *Opt. Express* 17, 264 (2009).
- 20. P. J. Shadbolt et al., Nat. Photonics 6, 45 (2011).
- E. Knill, R. Laflamme, G. J. Milburn, *Nature* 409, 46 (2001).
- C. K. Hong, Z. Y. Ou, L. Mandel, Phys. Rev. Lett. 59, 2044 (1987).
- 23. P. P. Rohde, T. C. Ralph, Phys. Rev. A 85, 022332 (2012).
- 24. P. J. Mosley *et al.*, *Phys. Rev. Lett.* **100**, 133601 (2008).
- D. O. Kundys, J. C. Gates, S. Dasgupta, C. Gawith, P. G. R. Smith, *IEEE Photon. Technol. Lett.* 21, 947 (2009).
- 26. Eq. 1 is expected to hold for any  $|S\rangle$  and  $|T\rangle$ ; however, the classical hardness of sampling P(S|T) is maximized when  $S_{j}$ ,  $T_{i} \in \{0,1\}$  for a given N and  $\Lambda$ .

- A. Laing, J. L. O'Brien (2012), http://arxiv.org/abs/ 1208.2868v1.
- A. Gilchrist, N. K. Langford, M. A. Nielsen, *Phys. Rev. A* 71, 062310 (2005).
- 29. P. P. Rohde, Phys. Rev. A 86, 052321 (2012).
- 30. T. Gerrits et al., Phys. Rev. A 84, 060301 (2011).
- 31. A. L. Migdall, D. Branning, S. Castelletto, *Phys. Rev. A* **66**, 053805 (2002)
- 32. J. Nunn et al. (2012), http://arxiv.org/abs/1208.1534v1.

Acknowledgments: We thank J. Nunn for valuable insights. This work was supported by the Engineering and Physical Sciences Research Council (EP/C013840/1, EP/H03031X/1, and EP/J000051/1), the European Commission project Q-ESSENCE (248095), the Royal Society, and the Air Force Office of Scientific Research (European Office of Aerospace Research and Development). X.M.J. and N.K.L. are supported by European Union Marie-Curie fellowships (PIIF-GA-2011-300820 and PIEF-GA-2010-275103). J.B.S. acknowledges support from the U.S. Air Force Institute of Technology. The views expressed in this article are those of the authors and do not reflect the official policy or position of the U.S. Air Force, Department of Defense, or the U.S. Government.

#### **Supplementary Materials**

www.sciencemag.org/cgi/content/full/science.1231692/DC1 Materials and Methods Supplementary Text References (33–37)

18 October 2012; accepted 3 December 2012 Published online 20 December 2012; 10.1126/science.1231692

## Observation of Radiation Pressure Shot Noise on a Macroscopic Object

T. P. Purdy, 1,2 R. W. Peterson, 1,2 C. A. Regal 1,2

The quantum mechanics of position measurement of a macroscopic object is typically inaccessible because of strong coupling to the environment and classical noise. In this work, we monitor a mechanical resonator subject to an increasingly strong continuous position measurement and observe a quantum mechanical back-action force that rises in accordance with the Heisenberg uncertainty limit. For our optically based position measurements, the back-action takes the form of a fluctuating radiation pressure from the Poisson-distributed photons in the coherent measurement field, termed radiation pressure shot noise. We demonstrate a back-action force that is comparable in magnitude to the thermal forces in our system. Additionally, we observe a temporal correlation between fluctuations in the radiation force and in the position of the resonator.

In measuring the trajectory of an object at the scale of our everyday experience, we rarely consider the fundamental limitations imposed by quantum mechanics. Yet quantum mechanical effects are present even when monitoring the position of macroscopic objects, and these effects are expected to soon limit, for example, the precision of gravitational wave observatories (*I*). Imagine measuring the position of an object to an accuracy  $\Delta x$ . A momentum uncertainty of at least  $\Delta p = \hbar/2\Delta x$  must then be present, where  $\hbar$  is the

momentum (or equivalently velocity) uncertainty adds position uncertainty at a later time. Thus, an observer must weigh pinpointing the location of the object against introducing quantum measurement back-action that obscures the subsequent motion.

For an optical position measurement, this

reduced Planck's constant that appears in the

Heisenberg uncertainty relation. This requisite

quantum back-action is termed radiation pressure shot noise (RPSN) (2, 3). A fluctuating force arises from, for instance, the recoil momentum transfer of randomly arriving photons (shot noise) reflecting off of an object. In the next-generation advanced gravitational wave observatories—such as the Laser Interferometer Gravitational Wave Observatory (LIGO) (1), Virgo, and the

Kamioka Gravitational Wave Detector (KAGRA) (4)—RPSN is predicted to limit sensitivity, even with test masses of tens of kilograms. Ideas developed to circumvent quantum limits imposed by back-action include quadrature-squeezed light (5) and back-action evasion techniques (4, 6). However, for typical objects, the scale of quantum back-action is small compared with thermal motion or classical probing noise. In this Report, we observe RPSN on a solid macroscopic (visible to the naked eye) mechanical resonator by using an optical interferometric measurement of its vibrational motion.

Figure 1A shows the canonical picture of a Heisenberg-limited continuous position measurement. The point at which the sum of the shot noise measurement imprecision (dashed line) and RSPN-induced displacement fluctuations (solid black line) are minimized is termed the standard quantum limit (SQL) (7, 8). Here, the displacement spectral density from RPSN at the mechanical resonance frequency,  $\omega_{\rm m}$ , is  $S_z^{SQL}(\omega_{\rm m}) =$  $\hbar/m\omega_{\rm m}\Gamma_{\rm m}$ , where m and  $\Gamma_{\rm m}$  are the resonator's mass and damping rate, respectively. This fundamental scale is equivalent to one-half of the resonator's quantum mechanical zero point motion,  $Z_{zp}$ . We also define  $P^{SQL}$ , the power required for a shot noise-limited measurement imprecision of  $S_z^{SQL}(\omega_m)$ . Even with other mechanical noise sources present [e.g., thermal motion (solid brown line in Fig. 1A)], quantum back-action may still play an important role if the optical power, P, is sufficiently larger than  $P^{SQL}$ .

Whereas shot noise is a ubiquitous measurement limitation, experimental signatures of RPSN

<sup>&</sup>lt;sup>1</sup>JILA, University of Colorado and National Institute of Standards and Technology, Boulder, CO 80309, USA. <sup>2</sup>Department of Physics, University of Colorado, Boulder, CO 80309, USA.

<sup>\*</sup>To whom correspondence should be addressed. E-mail: tpp@iila.colorado.edu

on solid objects have remained elusive. Mechanical effects of photon recoil are routinely studied in atomic physics [(9) and references therein], and a RPSN observation analogous to ours has been made using a dilute gas of ultracold atoms (10). A promising route to studying RPSN in solid objects involves experiments that achieve high optomechanical coupling to high-frequency, small (nanometer- to centimeter-scale) mechanical resonators. Using such resonators, groups have initiated searches for RPSN (11, 12), observed classical analogs of RPSN (13), and predicted experimental signatures of RPSN (14-16). Back-action on a nanomechanical resonator has also been observed with the use of other measurement devices. such as single-electron transistors (17). Resonators have even been cooled with electromagnetic radiation to near their motional ground state, illustrating the capacity for dominant coherent optical forces (18–20). In these experiments, quantum back-action has thus far been limited to the scale of  $Z_{zp}$ , whereas in this Report, we demonstrate a strong back-action heating effect from RPSN. Additionally, in near-ground-state cooling experiments, correlations between shot noise and RPSN-driven mechanical motion are an important component of the observed optical spectra (21) and are responsible for the sideband asymmetry observed in (22).

Our optomechanical system consists of a silicon nitride membrane resonator inside of a Fabry-Perot optical cavity that is specially designed to operate at cryogenic temperatures (Fig. 1C) (23). Thompson et al. have shown that membrane motion can be coupled to a cavity through a dispersive interaction, where the cavity resonance frequency shifts as the membrane moves along the optical standing wave (24). This interaction imprints phase and amplitude modulation on transmitted laser light, allowing for readout of the membrane motion. In conjunction, the laser applies an optical gradient force to the membrane, pushing it toward higher optical intensity. Our membrane is a highly tensioned square plate with a 0.5-mm side length, 40-nm thickness, and an effective mass of ~7 ng. We operate in a helium flow cryostat with the resonator at a base temperature of 4.9 K, where intrinsic mechanical linewidths,  $\Gamma_0/2\pi$ , are typically less than 1 Hz. For the (2,2) mode oscillating at  $\omega_m/2\pi = 1.55$  MHz, we achieve a maximum single-photon optomechanical coupling rate  $g/2\pi = 16$  Hz.

We use two laser beams derived from the same 1064-nm source, both coupled to the same spatial mode of the cavity, but with orthogonal polarizations (Fig. 1C) (13, 14). The half-planar, 5.1-mm-long cavity has a full linewidth  $\kappa/2\pi \sim 1$  MHz, which varies slightly with the membrane position. The high-intensity "signal" beam is actively stabilized to the optical resonance. This beam provides the RPSN, and its transmitted intensity fluctuations constitute a record, which is partially obscured by optical loss, of the optical force on the resonator. The corresponding sensitive position measurement is wholly imprinted

in the unrecorded phase quadrature. Additional phase noise from fluctuations in the cavity-laser detuning precludes shot noise—limited phase-quadrature detection (23). The much weaker "meter" beam is tuned to the red of the optical resonance im-

printing the resonator's displacement spectrum on its transmitted intensity. Although its shot noise drive is much smaller, the meter beam provides optical Raman sideband cooling of the mechanical mode (25) to 1.7 mK. The optical damping

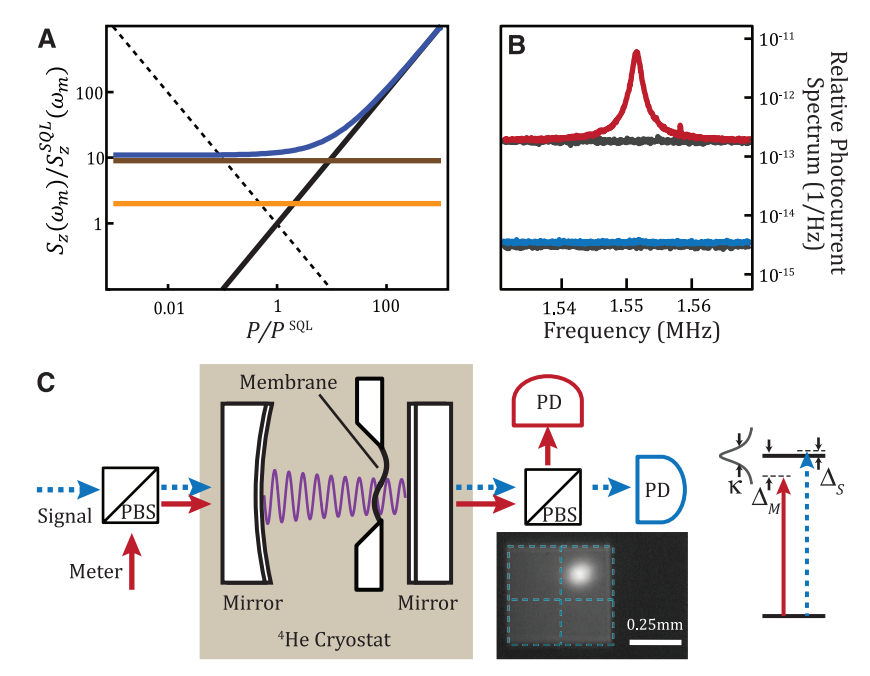
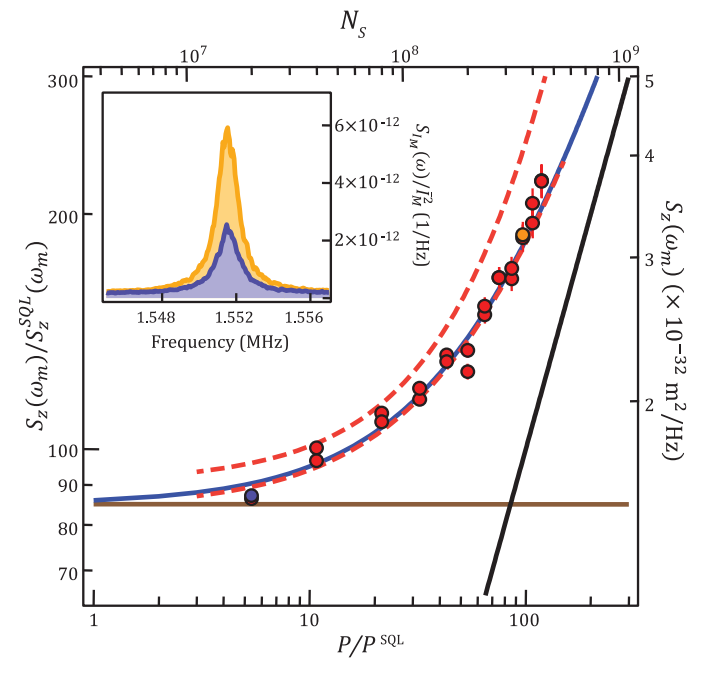


**Fig. 1.** (**A**) Canonical picture of continuous position measurement. RPSN (black), thermal motion (brown), and zero point motion (orange) combine to give the expected measurement result (blue). The dashed line represents the effective displacement noise from the shot noise—limited imprecision of an optical measurement. (**B**) Photocurrent spectra. The photocurrent spectral densities  $S_{I_S}(\omega)\bar{I}_S^2$  (blue) and  $S_{I_M}(\omega)\bar{I}_M^2$  (red), as well as the noise floors, including detector noise and the dominant shot noise (gray), are shown. (**C**) Experimental setup. Beams are combined and separated with polarizing beam splitters (PBS) and detected directly on photodetectors (PD). The inset photograph shows an in situ image of the square membrane and optical mode spot, with blue dashed lines indicating the nodes of the (2,2) mechanical mode. The inset diagram at right shows laser-cavity detunings.

Fig. 2. Displacement spectrum measurements. Measured peak displacement spectral density (circles), thermal contribution (brown line), and expected RPSN contribution (black line) are shown. The blue curve represents the theoretical prediction for the sum of thermal motion and RPSN, and the dashed red curves are bounds on theoretical estimates, including systematic uncertainty in device parameters and the classical noise contribution. Device parameters:  $q/2\pi =$ 16.1  $\pm$  0.3 Hz,  $\kappa/2\pi$  = 0.89 MHz,  $\Delta_{\rm S}/2\pi$  = 2.0  $\pm$ 0.5 kHz,  $\Delta_{\rm M}/2\pi = 0.7$  MHz,  $N_{\rm M} = 7.0 \pm 0.3 \times 10^6$  $\omega_{\rm m}/2\pi = 1.551 \, {\rm MHz},$  $\Gamma_0/2\pi = 0.47$  Hz, and  $\Gamma_{\rm m}/2\pi=$  1.43 kHz. (Inset)



Transmission spectra for  $R_S = 0.056$  (blue) and  $R_S = 1.0$  (orange), with corresponding points in the main plot highlighted in blue and orange.

greatly eases the requirements on the signal-beamcavity detuning due to both parametric instabilities at positive detuning and the contamination of cross-correlation by thermal motion (12, 15, 26), but it does not change the sensitivity of the resonator to RPSN relative to thermal forces.

The effect of the optomechanical coupling on the resonator from a single laser (25, 27) or multiple beams (15) has been well studied. The resonator's mechanical susceptibility is modified to include optomechanical damping and frequency shifts from each laser. Additionally, the effective phonon occupation,  $n_{\rm m}$ , is modified. The optomechanical damping cools the resonator; RPSN increases the amplitude of motion. In equilibrium, a simple rate equation gives  $n_{\rm m}$  =  $(n_{\rm th}\Gamma_0 + n_{\rm S}\Gamma_{\rm S} + n_{\rm M}\Gamma_{\rm M})/\Gamma_{\rm m}$ . Here,  $n_{\rm th}$  is the thermal phonon occupation;  $n_S$  and  $\Gamma_S$  (or  $n_M$  and  $\Gamma_{\rm M}$ ) are the effective bath temperature and optomechanical damping rate of the signal (or meter) laser. The total mechanical damping rate is  $\Gamma_{\rm m}$  =  $\Gamma_0 + \Gamma_S + \Gamma_M$ . In our experiments  $\Gamma_M >> \Gamma_0$  and  $\Gamma_{\rm S}$ , whereas  $\Delta_{\rm S} \sim 0$  and  $N_{\rm S} >> N_{\rm M}$ , where  $\Delta_{\rm S}$  and  $N_{\rm S}$  (or  $\Delta_{\rm M}$  and  $N_{\rm M}$ ) are the laser-cavity detuning and intracavity photon occupation of the signal (or meter) beam. RPSN dominates over thermal noise when the ratio of radiation to thermal forces  $R_{\rm S} = (C_{\rm S}/n_{\rm th})[1 + (2\omega_{\rm m}/\kappa)^2]^{-1} >$ 1, where  $C_S = 4N_S g^2 / \kappa \Gamma_0$  is the multiphoton cooperativity. We are able to reach this highcooperativity regime ( $C_{\rm S} \sim 10^6$ ) due to the small mass, weak intrinsic damping, and cryogenic environment of our resonator.

The increase in phonon occupation resulting from RPSN is shown in Fig. 2. The meter beam transmission spectrum,  $S_{I_{M}}(\omega)$  (Fig. 2, inset), shows a marked increase in spectral area, or equivalently,  $n_{\rm m}$  as the measurement strength is increased to where  $R_{\rm S} \sim 1$ . Here, the employed  $N_{\rm S} = 3.6 \times 10^8$  is equivalent to ~200  $\mu$ W of detected optical power. The device shows good agreement with a theory of measurement backaction (Fig. 2, blue curve) based on independently measured device parameters. Because a separate meter beam is used to read out the mechanical motion, the measurement noise floor associated with these data are independent of the shot noise level of the signal beam, as depicted by the dashed line in Fig. 1A. The increased spectral density also includes a small contribution from classical radiation pressure noise. Taking into account the thermal motion and classical laser intensity noise, we can attribute at least 40% of the total displacement spectrum to RPSN at the maximum signal beam strength. We have also measured similar back-action heating on another device with smaller  $\Gamma_0$  and lower classical intensity noise (fig. S5). The dashed curves of Fig. 2 represent bounds on the expected spectral densities accounting for systematic uncertainties in the device parameters and classical noise level (26). Another effect that might mimic RPSN is physical heating. To test for physical heating, we monitor the temperature of a higher-frequency, weakly optomechanically coupled mechanical mode where RSPN is negligible. We do not ob-

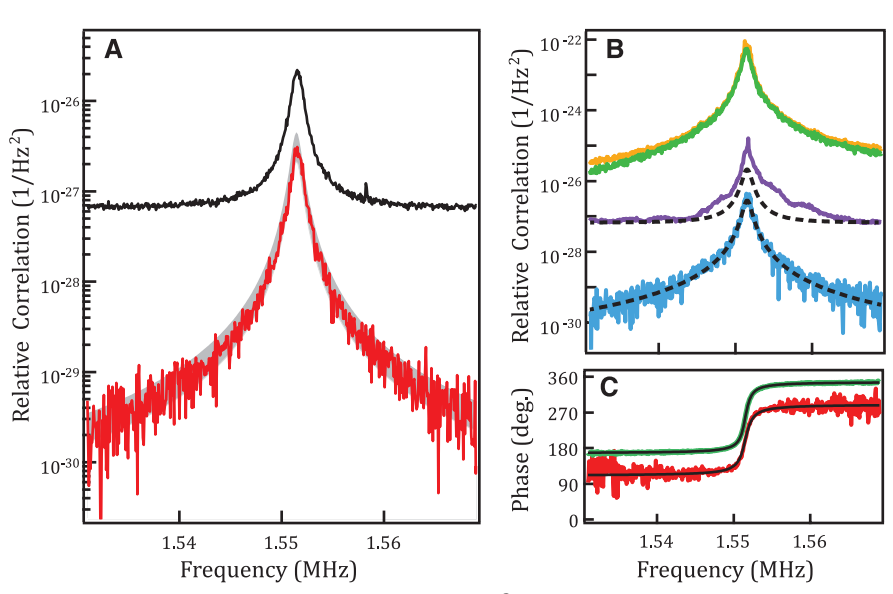


**Fig. 3.** Cross-correlation measurements. **(A)**  $|S_{I_{SM}}(\omega)\bar{I}_I\bar{S}_M^{-1}|^2$  measured (red) and expected, including systematic uncertainty (gray), and  $S_{I_S}(\omega)\bar{I}_S^2\times S_{I_M}(\omega)\bar{I}_M^2$  (black). Parameters are as listed in the Fig. 2 caption, except  $\Delta_S/2\pi=300\pm100$  Hz,  $g/2\pi=14.8\pm0.4$  Hz, and  $N_S=3.2\times10^8$ . The resolution bandwidth is 50 Hz. **(B)**  $|S_{I_{SM}}(\omega)\bar{I}_S^2I_M|^2$  (green) and  $S_{I_S}(\omega)\bar{I}_S^2\times S_{I_M}(\omega)\bar{I}_M^2$  (orange), where classical intensity noise at the level of ~40 times the shot noise is added to the signal beam, raising the overall signal levels by the same factor.  $|S_{I_{SM}}(\omega)\bar{I}_S^2I_M|^2$  (blue) and  $S_{I_S}(\omega)\bar{I}_S^2\times S_{I_M}(\omega)\bar{I}_M^2$  (purple), where the membrane is driven with excess mechanical noise. Fits to the data from (A) are displayed for reference (dashed black curves), showing that despite increased mechanical motion (purple curve above the top dashed curve), the correlation remains unchanged (blue curve coinciding with the lower dashed curve). **(C)** Phase of the cross-correlation, with classical intensity noise on signal beam (green) and without added noise (red). Black curves are fits to the data.

serve a large response from this mode, which indicates that the absorbed laser light causes a <10% increase in the bath temperature (fig. S4).

We next examine the temporal correlations between the signal and meter beam photocurrents (14, 15). We compute the spectrum of the two-time cross-correlation function  $S_{I_{SM}}(\omega) =$  $\langle I_{\rm S}^*(\omega)I_{\rm M}(\omega)\rangle$ , where  $I(\omega)$  is the complex Fourier transform of the photocurrent I(t), and the angle brackets represent an average over many realizations of the experiment. Thermal and other ambient motion, as well as measurement noise uncorrelated to the radiation pressure drive, are rejected by this technique, making it a powerful tool in understanding RPSN. In the limit  $\Gamma_m \ll \kappa$ , the correlation should reflect the Lorentzian response function of the optically damped resonator, driven by the locally white shot noise. In Fig. 3A, we show a cross-correlation measurement and, for reference, the product spectrum,  $S_{I_{\rm S}}(\omega) \times S_{I_{\rm M}}(\omega)$ .  $S_{I_{\rm S}}(\omega)$  and  $S_{I_{\rm M}}(\omega)$  for these data are shown in Fig. 1B. If the two beams are perfectly correlated, the cross-correlation and product spectra should coincide. However, an uncorrelated measurement background, dominated by the meter's shot noise and thermal motion, appears only on the product spectrum. Additionally, the imperfect detection efficiency leads to a loss of correlation. We measure a peak normalized correlation (the ratio of the red to black curve peaks in Fig. 3A) of  $C(\omega_{\rm m}) =$  $|S_{I_{SM}}(\omega_{\rm m})|^2/S_{I_{\rm S}}(\omega_{\rm m})S_{I_{\rm M}}(\omega_{\rm m}) = 0.14$ . An estimate, ignoring classical noise and assuming  $\Delta_S = 0$ , is given by  $C(\omega_{\rm m}) = R_{\rm S}/(1 + R_{\rm S}) \times \kappa_{\rm R}/\kappa \times \varepsilon_{\rm S} =$  $0.15 \pm 0.02$ , where  $R_S/(1 + R_S) = 0.40 \pm 0.03$  is the fraction of  $S_z(\omega_m)$  due to RPSN,  $\kappa_R/\kappa = 0.59$ is the fraction of the light through the output port, and  $\varepsilon_S = 0.63 \pm 0.03$  is the postcavity detection efficiency. By intentionally adding classical intensity noise that is much larger than shot noise to the signal laser, we demonstrate a (classical) normalized cross-correlation that approaches unity (Fig. 3B).

Figure 3C shows the phase of the correlation both with and without large classical intensity noise on the signal beam. Both show the 180° phase shift expected from the mechanical response. Importantly, we also expect a phase offset of arctan( $2\omega_{\rm m}/\kappa$ ) between the classical noise—dominated drive and the shot noise—dominated drive (15, 26). Measurements of this phase offset imply that 75% of the radiation pressure drive is from shot noise, in agreement with the directly measured classical noise range in  $S_{I_{\kappa}}(\omega)$ .

If  $\Delta_{\rm S}$  is not zero, the cross-correlation will be distorted. Mechanical motion transduced directly onto  $I_{\rm S}$  may constructively or destructively add to the RPSN correlation, depending on the sign of  $\Delta_{\rm S}$ . By fitting the correlation data to the expected line shape (26), we estimate  $\Delta_{\rm S} = 0.0003 \, {\rm K}$ , implying only a 3% contribution to  $S_{I_{\rm SM}}(\omega_{\rm m})$  from thermal motion. We have also performed an experimental test to demonstrate the rejection of ambient motion from the cross-correlation spectrum (Fig. 3B). Here, we mechanically excite

the membrane with a white noise—driven piezoelectric actuator (purple trace exceeds dashed curve in Fig. 3B), which also drives mechanical modes of the mirrors and supports, leading to extra modulation. However, the cross-correlation spectrum (blue trace) remains unchanged, equal to the unperturbed spectrum (dashed curve), implying that very little of the ambient motion is transduced.

The cross-correlation can also be viewed as evidence that we have made a quantum nondemolition (QND) measurement of the intracavity photon fluctuations of the signal beam (14, 28). Here, the membrane acts as the measurement device, with its state of motion recording the photon fluctuations over the band of the mechanical resonance. The correlation C is equivalent to a state preparation fidelity for a nonideal QND measurement (29). Further, it has been shown that frequency-dependent ponderomotive squeezing of the signal beam quantum noise is possible (30)and has recently been demonstrated in an atomic gas cavity optomechanical system (31). For our current laser configuration ( $\Delta_S = 0$ ), we do not expect to see squeezing in the detected amplitude quadrature. However, our device parameters are sufficient to realize much stronger squeezing than has previously been demonstrated, limited mainly by optical loss. Our observations open the door to realizing position measurement near the SQL if residual thermal noise and excess cavity-laser phase noise can be eliminated with improved devices or a colder base temperature.

#### References and Notes

- 1. G. M. Harry, Class. Quantum Gravity 27, 084006 (2010).
- 2. V. Braginsky, S. Vyatchanin, Sov. Phys. JETP 47, 433 (1978).
- 3. C. M. Caves, Phys. Rev. D Part. Fields 23, 1693 (1981).
- K. Somiya, Class. Quantum Gravity 29, 124007 (2012).
   H. J. Kimble, Y. Levin, A. B. Matsko, K. S. Thorne,
- S. P. Vyatchanin, *Phys. Rev. D Part. Fields* **65**, 022002 (2001). 6. V. B. Braginsky, Y. I. Vorontsov, K. S. Thorne, *Science*
- V. B. Braginsky, Y. I. Vorontsov, K. S. Thorne, *Science* 209, 547 (1980).
- J. D. Teufel, T. Donner, M. A. Castellanos-Beltran,
   W. Harlow, K. W. Lehnert, Nat. Nanotechnol. 4, 820 (2009).
- 8. G. Anetsberger et al., Phys. Rev. A 82, 061804 (2010).
- D. M. Stamper-Kurn, in *Cavity Optomechanics*, M. Aspelmeyer,
   T. Kippenberg, F. Marquardt, Eds. (Springer, New York);
   preprint available at http://arxiv.org/abs/1204.4351.
- K. W. Murch, K. L. Moore, S. Gupta, D. M. Stamper-Kurn, Nat. Phys. 4, 561 (2008).
- 11. I. Tittonen et al., Phys. Rev. A 59, 1038 (1999).
- 12. P. Verlot et al., C. R. Phys. 12, 826 (2011).
- P. Verlot, A. Tavernarakis, T. Briant, P.-F. Cohadon,
   A. Heidmann, *Phys. Rev. Lett.* **102**, 103601 (2009).
- A. Heidmann, Y. Hadjar, M. Pinard, Appl. Phys. B 64, 173 (1997).
- 15. K. Børkje et al., Phys. Rev. A 82, 013818 (2010).
- 16. K. Yamamoto et al., Phys. Rev. A 81, 033849 (2010).
- 17. A. Naik et al., Nature 443, 193 (2006).
- 18. ]. D. Teufel et al., Nature 475, 359 (2011).
- 19. J. Chan et al., Nature 478, 89 (2011).
- E. Verhagen, S. Deléglise, S. Weis, A. Schliesser,
   T. J. Kippenberg, *Nature* 482, 63 (2012).

- 21. F. Y. Khalili et al., Phys. Rev. A 86, 033840 (2012).
- A. H. Safavi-Naeini et al., Phys. Rev. Lett. 108, 033602 (2012).
- T. P. Purdy, R. W. Peterson, P.-L. Yu, C. A. Regal, New I. Phys. 14, 115021 (2012).
- 24. J. D. Thompson et al., Nature 452, 72 (2008).
- F. Marquardt, J. P. Chen, A. A. Clerk, S. M. Girvin, *Phys. Rev. Lett.* 99, 093902 (2007).
- Materials and methods are available as supplementary materials on Science Online.
- I. Wilson-Rae, N. Nooshi, W. Zwerger, T. J. Kippenberg, *Phys. Rev. Lett.* 99, 093901 (2007).
- K. Jacobs, P. Tombesi, M. J. Collett, D. F. Walls, *Phys. Rev. A* 49, 1961 (1994).
- M. J. Holland, M. J. Collett, D. F. Walls, M. D. Levenson, *Phys. Rev. A* 42, 2995 (1990).
- 30. C. Fabre et al., Phys. Rev. A 49, 1337 (1994).
- 31. D. W. C. Brooks et al., Nature 488, 476 (2012).

Acknowledgments: We thank P.-L. Yu for technical assistance and K. Lehnert's group for helpful discussions. This work is supported by: the Defense Advanced Research Projects Agency Quantum-Assisted Sensing and Readout program, the Office of Naval Research Young Investigator Program, and the JILA NSF Physics Frontier Center. T.P.P. thanks the National Research Council for support. C.A.R. thanks the Clare Boothe Luce foundation for support.

#### Supplementary Materials

www.sciencemag.org/cgi/content/full/339/6121/801/DC1 Materials and Methods

Figs. S1 to S5

References (32, 33)

9 October 2012; accepted 18 December 2012 10.1126/science.1231282

# Similarity of Scattering Rates in Metals Showing *T*-Linear Resistivity

J. A. N. Bruin, H. Sakai, R. S. Perry, A. P. Mackenzie

Many exotic compounds, such as cuprate superconductors and heavy fermion materials, exhibit a linear in temperature (T) resistivity, the origin of which is not well understood. We found that the resistivity of the quantum critical metal  $Sr_3Ru_2O_7$  is also T-linear at the critical magnetic field of T. Using the precise existing data for the Fermi surface topography and quasiparticle velocities of  $Sr_3Ru_2O_7$ , we show that in the region of the T-linear resistivity, the scattering rate per kelvin is well approximated by the ratio of the Boltzmann constant to the Planck constant divided by T. Extending the analysis to a number of other materials reveals similar results in the T-linear region, in spite of large differences in the microscopic origins of the scattering.

hen the high-temperature cuprate superconductors were discovered, it quickly became clear that the highest superconducting transition temperatures were seen in materials whose electrical resistivity varied linearly with temperature (*T*) in certain regions of the temperature-doping phase diagram. Since then, *T*-linear resistivity has been seen in the pnictide and organic superconductors, as well as in many heavy fermion compounds, both superconducting and non-superconducting. In most of the heavy fermion materials, the *T*-linear resistivity is seen when they have been tuned by some external

<sup>1</sup>Scottish Universities Physics Alliance, School of Physics and Astronomy, University of St Andrews, North Haugh, St Andrews KY16 9SS, UK. <sup>2</sup>Scottish Universities Physics Alliance, School of Physics and Astronomy, University of Edinburgh, Mayfield Road, Edinburgh EH9 3JZ, UK. parameter to create a low-temperature continuous phase transition known as a quantum critical point (QCP). *T*-linear resistivity is therefore often associated with quantum criticality. However, other power laws—for example, *T*<sup>1.5</sup>—are also seen in the resistivity in quantum critical systems (*I*), and the origin of the *T*-linear term remains the subject of active research and debate. Here, we present an analysis of electrical transport data from 1.5 to 400 K in Sr<sub>3</sub>Ru<sub>2</sub>O<sub>7</sub> and compare our findings to those in a wide variety of other materials, including elemental metals, that exhibit *T*-linear resistivity.

 $\rm Sr_3Ru_2O_7$  is a magnetic-field—tuned quantum critical system (2) that can be prepared in single-crystal form with very low levels of disorder (3, 4). For an applied field oriented parallel to the crystallographic c axis, the approach to the quantum

critical point at the critical field  $\mu_0 H_c = 7.9 \text{ T}$  is cut off by the formation of a purity-sensitive nematic phase for 7.8 T  $< \mu_0 H <$  8.1 T and T < 1.2 K. Outside this phase, canonical signatures of quantum criticality are seen in a range of physical properties including the spin-lattice relaxation rate, thermal expansion, specific heat, and magnetocaloric effect (5-8). As the magnetic field is varied at low temperature, both the specific heat and entropy show a strong peak, centered on  $H_c$ . Cooling at zero field shows a broad peak in the electronic specific heat coefficient  $\gamma = c_{\rm el}/T$ , centered at approximately 10 K but extending to  $T^* \sim 25$ K. As the field is increased, this peak sharpens, and its characteristic temperature is depressed, until at  $H_c$ ,  $\gamma$  varies as  $-\ln T$  for 1.2K < T < 20 K. At all fields, an entropy of  $\sim 0.1R \ln 2$  is recovered by  $T^*$ , where R is the molar gas constant (8). These observations indicate that the ~25K energy scale is associated with a fraction of the states in the Brillouin zone and that these states are responsible for the quantum criticality. Above  $T^*$ , they have the entropic characteristics of "classical" fluctuators at all applied fields, with the crossover temperature suppressed on the approach to  $H_c$ .

The fact that only some of the states in the Brillouin zone participate thermodynamically in the quantum criticality is consistent with findings from the de Haas-van Alphen (dHvA) effect and angle-resolved photoemission (9, 10). Six distinct dHvA frequencies are identified, each corresponding to quasi–two dimensional (2D) Fermi surface pockets, and the quasiparticle masses are essentially field-independent for five of them (9). Thermo-



### Observation of Radiation Pressure Shot Noise on a Macroscopic Object

T. P. Purdy, R. W. Peterson and C. A. Regal

Science **339** (6121), 801-804. DOI: 10.1126/science.1231282

**Macroscopic Uncertainty** 

According to the Heisenberg uncertainty principle, it is impossible to know both the position and the momentum of a microscopic particle with absolute certainty; pinpointing the location introduces an uncertainty in the velocity, which translates into position uncertainty at later times. Now, **Purdy et al.** (p. 801; see the Perspective by **Milburn**) have measured the position of a macroscopic object (a small, but visible-to-the-naked-eye membrane suspended in an optical cavity) at cryogenic temperatures and observed the uncertainty in its position caused by the recoiling photons used for the measurement.

ARTICLE TOOLS http://science.sciencemag.org/content/339/6121/801

SUPPLEMENTARY http://science.sciencemag.org/content/suppl/2013/02/13/339.6121.801.DC2
MATERIALS http://science.sciencemag.org/content/suppl/2013/02/13/339.6121.801.DC2

http://science.sciencemag.org/content/suppl/2013/02/13/339.6121.801.DC1

RELATED http://science.sciencemag.org/content/sci/339/6121/770.full

http://science.sciencemag.org/content/sci/339/6121/861.2.full

**REFERENCES** This article cites 31 articles, 1 of which you can access for free

http://science.sciencemag.org/content/339/6121/801#BIBL

PERMISSIONS http://www.sciencemag.org/help/reprints-and-permissions

Use of this article is subject to the Terms of Service